



Gas/water foams stabilized with a newly developed anionic surfactant for gas mobility control applications

Mohammed A. Almobarky¹ · Zuhair AlYousif² · David Schechter³

Received: 17 March 2019 / Published online: 7 April 2020
© The Author(s) 2020

Abstract

Carbon dioxide (CO₂) flooding is one of the most globally used EOR processes to enhance oil recovery. However, the low gas viscosity and density result in gas channeling and gravity override which lead to poor sweep efficiency. Foam application for mobility control is a promising technology to increase the gas viscosity, lower the mobility and improve the sweep efficiency in the reservoir. Foam is generated in the reservoir by co-injection of surfactant solutions and gas. Although there are many surfactants that can be used for such purpose, their performance with supercritical CO₂ (ScCO₂) is weak causing poor or loss of mobility control. This experimental study evaluates a newly developed surfactant (CNF) that was introduced for ScCO₂ mobility control in comparison with a common foaming agent, anionic alpha olefin sulfonate (AOS) surfactant. Experimental work was divided into three stages: foam static tests, interfacial tension measurements, and foam dynamic tests. Both surfactants were investigated at different conditions. In general, results show that both surfactants are good foaming agents to reduce the mobility of ScCO₂ with better performance of CNF surfactant. Shaking tests in the presence of crude oil show that the foam life for CNF extends to more than 24 h but less than that for AOS. Moreover, CNF features lower critical micelle concentration (CMC), higher adsorption, and smaller area/molecule at the liquid–air interface. Furthermore, entering, spreading, and bridging coefficients indicate that CNF surfactant produces very stable foam with light crude oil in both deionized and saline water, whereas AOS was stable only in deionized water. At all conditions for mobility reduction evaluation, CNF exhibits stronger flow resistance, higher foam viscosity, and higher mobility reduction factor than that of AOS surfactant. In addition, CNF and ScCO₂ simultaneous injection produced 8.83% higher oil recovery than that of the baseline experiment and 7.87% higher than that of AOS. Pressure drop profiles for foam flooding using CNF was slightly higher than that of AOS indicating that CNF is better in terms of foam–oil tolerance which resulted in higher oil recovery.

Keywords Supercritical CO₂ foam · Foam mobility control · Foam flooding · Enhanced oil recovery (EOR) · Foam assisting CO₂ EOR

Edited by Yan-Hua Sun

- ✉ Mohammed A. Almobarky
mmobarky@ksu.edu.sa
- ✉ Zuhair AlYousif
Zuhair.Yousif@aramco.com

- ¹ Department of Petroleum and Natural Gas Engineering, College of Engineering, King Saud University, Riyadh, Kingdom of Saudi Arabia
- ² Saudi Aramco, Dhahran, Kingdom of Saudi Arabia
- ³ Harold Vance Petroleum Engineering Department, Texas A&M University, College Station TX, USA

1 Introduction

It is estimated that two-thirds of the original oil in place (OOIP) are left underground after the primary and secondary oil recovery processes (Green and Willhite 1998). For tertiary recovery, many enhanced oil recovery (EOR) methods can be used to extract more oil from reservoirs. Among these EOR methods, CO₂ injection is one the most used processes globally (Taber et al. 1997). However, gas injection processes face many challenges such as gas channeling and gravity override that lead to poor sweep efficiency (Healy et al. 1994). Many techniques have been applied to enhance the sweep efficiency such as water alternating gas (WAG), polymer, and foam. Foam is a promising technology that can be used to reduce the mobility of the injected gas by

increasing its viscosity (Enick et al. 2012) and diverting the flow toward lower permeability zones where the remaining oil exists (Fried 1961).

Surfactants are the main component in a foam system. They facilitate the foam generation by reducing the gas–water interfacial tension and adsorb at the interfaces to make the foam with the required stability by stabilizing the thin films between bubbles (Schramm 2000). Thus, the surfactant screening is the first step toward a successful foam project (Boeije et al. 2017). In foam applications, in general, and particularly in CO₂ EOR, the surfactant structure is a significant factor that affects the efficiency in every aspect of the process: gas viscosity, mobility control, and EOR (Adkins et al. 2010). These effects are related to different interactions of surfactants and CO₂ (Adkins et al. 2010). Moreover, the presence of supercritical CO₂ (ScCO₂) results in low pH acidic environment where some types of surfactants hydrolyze and lose their interfacial activity such as sulfates (Talley 1988).

Alpha olefin sulfonate (AOS) is hydrolytically and thermally stable, and soluble at low to medium hard water (Porter 1994). Farajzadeh et al. (2010) experimentally investigated the use of AOS for mobility control and EOR in miscible and immiscible flooding with the aid of CT scanner for simultaneous monitoring of the flooding process. They reported 19% more oil recovery with ScCO₂ than that of the immiscible CO₂ flooding. However, no sharp front was observed with the use of ScCO₂. They attributed this to the poor foam stability with oil. Haugen et al. (2012) experimentally used AOS for mobility control and EOR in fractured oil wet and water wet cores and reported that the pre-generated foam is better than in situ foam generation in terms of mobility reduction and oil recovery. They attributed the results to the poor foam–oil tolerance. Li et al. (2012) used AOS in surfactant-alternating-gas (SAG) injection mode for foam generation using N₂. Their experiments were conducted on a two-dimensional sand pack with 19–1 permeability contrast. They attributed the poor sweep efficiency to the weak foam stability in the presence of crude oil. They suggested that enhancing the foam–oil tolerance could provide higher oil recovery because this may enhance the sweep efficiency. Indeed, mixing the surfactant with a foam booster CTAB zwitterionic surfactant improved the foam–oil tolerance,

provided better displacement efficiency, and resulted in higher oil recovery.

The aim of this study is to evaluate the ability of a newly developed anionic surfactant (CNF) to control the mobility of ScCO₂. Moreover, the performance of CNF is compared with C_{14–16} AOS (anionic surfactant) which is one of the most widely used in literature with CO₂ in gaseous and supercritical states. This newly developed surfactant and the major challenges for its utilization with ScCO₂ may provide more opportunities for foam applications in foam-assisting miscible CO₂ EOR projects.

2 Experimental materials

Table 1 shows the general properties of both surfactants used in experimental work. Surfactants were diluted with deionized (DI) water (ASTM, type II) provided by LabChem Inc. Moreover, tests were conducted at 0.5 wt% surfactant concentration. Besides deionized water, the salinity effect was investigated using brine solutions (NaCl solutions) at 10,000, 20,000, and 30,000 ppm (NaCl was purchased from Cole-Parmer). The crude oil used in this study was from North Burbank Unit, OK, USA (NBU). It is light crude oil with API gravity of 33.7° and viscosity of 8 cP at room temperature of 23 °C, and 39.5° API and 3.27 cP at 50 °C which is the reservoir temperature. The glass-bead pack was made using glass beads with a specific gravity of 2.5 and a diameter of 100 μm, which were purchased from Potters Industries LLC.

3 Methodology

The experimental work was divided into three stages: static foam tests, interfacial tension measurements, and dynamic foam tests. The dynamic foam tests were divided into three sections: mobility reduction evaluation in the high-permeability glass-bead pack, mobility reduction evaluation in low-permeability Bentheimer sandstone cores, and core flooding experiments. The surfactant concentrations were constant at 0.5 wt%, diluted with deionized water, and prepared

Table 1 Properties of the surfactants

Surfactant	Form	Chemical family	pH	Density, g/mL	Charge	Flash point, °C	Carbon chain length
CNF	Liquid	Alpha olefin sulfonate, isopropyl alcohol, and citrus terpenes	7.73	1.07	Anionic	> 93.3	–
AOS	Liquid	Alpha olefin sulfonate	8.20	1.06	Anionic	> 94.0	14–16

with NaCl solutions of three salinities: 10,000, 20,000, and 30,000 ppm.

3.1 Static foam tests

Foam was generated by shaking 3 mL of surfactant solutions in 13 × 100-mm (9-mL) Pyrex glass test tubes. Care has been taken to perform 10–15 gentle and uniform shakings for all samples. Samples were prepared at 0.5 wt% concentration in deionized water, 10,000, 20,000, and 30,000 NaCl solutions. After the foam has been generated with shaking inside the test tube, the foam columns were monitored by taking images at different times. Then, the foam column lengths were measured from images using ImageJ software. The foaming ability was investigated using the initial foam column length (h_{fi}), and the foam stability was measured by the foam half-life (FHL), $t_{1/2}$, which is the time at which the foam column loses half of the initial foam column length h_{fi} . The samples were prepared for static tests without oil and stirred for about 12 h before testing. For static tests with crude oil, the samples were prepared at 0.5 wt% surfactant concentration and stirred for 12 h, and the surfactant solution was placed in 9-mL test tubes above which the crude oil was simply poured. Then, the sample was shaken immediately.

3.2 Interfacial tension measurements

Air–water surface tension measurements were conducted at different surfactant concentrations in DI water using a Data-physics OCA 15 Pro IFT instrument, pendant drop method. The surface measurements were used for critical micelle concentration (CMC) determination and interfacial activity predictions for both surfactants.

The air–water surface tension versus the logarithmic values of the surfactant concentrations below the CMC is a linear relationship. The slope of this straight line can be used to interpret the interfacial activities: adsorption and area/molecule at the interface. According to the Gibbs adsorption equation, the higher the slope is, the higher the adsorption at the air–water interface. Furthermore, the higher the adsorption of surfactant molecules at the interface results in smaller area/molecule and stronger packing that induces higher foam stability (Rosen and Kunjappu 2004).

The interfacial tension measurements, also, can be also used to investigate the foam–oil tolerance by calculating the entering coefficient (E) (Robinson and Woods 1948), spreading coefficient (S) (Harkins 1941), bridging coefficient (B) (Denkov 2004), and the lamellae number (L) (Schramm and Novosad 1990) using Eqs. (1), (2), (3), and (4).

$$E = \sigma_{a/w} + \sigma_{o/w} - \sigma_{o/g} \tag{1}$$

$$S = \sigma_{a/w} - (\sigma_{o/w} + \sigma_{o/g}) \tag{2}$$

$$B = \sigma_{a/w}^2 + \sigma_{o/w}^2 - \sigma_{o/g}^2 \tag{3}$$

$$L = \frac{\sigma_{a/w}}{\sigma_{o/w}} \tag{4}$$

where $\sigma_{a/w}$, $\sigma_{o/w}$, $\sigma_{o/g}$ are the air–water, oil–water, and oil–gas interfacial tensions, respectively.

3.3 Dynamic foam tests

These experiments were designed for mobility reduction evaluation and oil recovery investigation by conducting core flood experiments.

3.3.1 Mobility reduction evaluation in the high-permeability glass-bead pack

These experiments were conducted at a high shear rate of 317 s⁻¹ and a low shear rate of 9.51 s⁻¹. Furthermore, three injection qualities 50%, 70%, and 90% were used. All experiments were conducted at 1800 psi and 50 °C to ensure the supercritical conditions of CO₂. The foam was generated by simultaneously injecting the surfactant solution and supercritical CO₂ (ScCO₂) through the glass-bead pack. The pressure drop was measured using two sets of pressure transducers: 500-psi for high range and 50-psi for low range. The pressure drop data were collected using a data acquisition system. The onset of a strong foam generation was recognized as a rapid increase in pressure drop according to Dickson et al. (2002). The flow continued with monitoring the pressure drop until the steady-state pressure drop across the glass-bead pack was reached. Then, the steady-state pressure data were averaged and used to calculate the mobility, foam effective viscosity, and mobility reduction factor (MRF) using the following equations.

$$\lambda = \frac{k}{\mu} = \frac{ql}{A\Delta P} \tag{5}$$

$$\mu_{\text{eff}} = \frac{k}{\lambda} \tag{6}$$

$$f_{\text{mr}} = \frac{\Delta P_{\text{foam}}}{\Delta P_{\text{baseline}}} \tag{7}$$

where λ is the mobility, k is the permeability, μ is the viscosity, q is the flow rate, l is the length of the porous media, A is the cross-sectional area of the glass-bead pack, ΔP is the pressure drop across the porous media, μ_{eff} is the foam effective viscosity, and f_{mr} is the mobility reduction factor.

Table 2 shows the dimensions and petrophysical properties of the glass-bead pack which was filled with 100 μm glass beads. Figure 1 shows the experimental setup for the mobility reduction evaluation.

The baseline experiment, in which ScCO_2 was injected without surfactant, was also conducted for comparison purposes. Detailed experimental conditions are described in Sect. 4.4.

3.3.2 Mobility reduction evaluation in low-permeability Bentheimer sandstone cores

All tests in this section were conducted on homogeneous Bentheimer sandstone cores (diameter, 1 in.; length, 12 in.). The core was left in an oven overnight for drying. Then, it was mounted in the core holder and 500 psi overburden pressure was applied. After that, the air was removed from the core using a vacuum pump followed by saturating the core with 10,000 ppm NaCl brine at which its pore volume (PV) and porosity can be measured. The system was then pressurized using the back-pressure regulator, as shown in Fig. 1. After the system was pressurized and the temperature was maintained at 50 $^\circ\text{C}$, the absolute permeability was measured by obtaining the pressure drop at different flow rates using Darcy's law. Then, 5–6 PV of brine were injected

to ensure 100% core saturation. Although the XRD tests for these rocks show that their composition is 100% quartz, 1 PV of the surfactant solution was injected into the core at 5 ft/day ($\sim 9 \text{ s}^{-1}$ shear rate) to mitigate the effect of surfactant adsorption on the rock surfaces. After that, the foam was applied by simultaneously injecting the surfactant solution and ScCO_2 or N_2 gas at 5 ft/day. The foam injection was continued until the steady pressure drop across the core was reached. The recorded steady-state pressure drop data were averaged and used to calculate the mobility, effective viscosity of foam, and MRF using Eqs. 5, 6, and 7.

Figure 1 above shows a schematic diagram of the experimental setup for mobility evaluation in sandstone cores. Properties of Bentheimer sandstone cores and experimental conditions for all runs are described in Sect. 4.5. Moreover, the last two runs listed (runs 9 and 10) are baseline experiments conducted using N_2 and ScCO_2 injection for comparison purposes, respectively. In all runs, the salinity of the surfactant solution or water injected is 10,000 ppm.

3.3.3 Core flooding experiments

The core flooding experiments were also conducted on homogeneous Bentheimer sandstone cores with a diameter of 1" and a length of 12". The core was left in an oven overnight for drying. Then, it was vacuumed and saturated with 10,000 ppm brine at which the pore volume and porosity were measured. After that, 5–6 PV of 10,000 ppm brine were injected into the core at 5 ft/day to ensure that the core sample was 100% water-saturated. Then, the absolute permeability was calculated using Darcy's law. The setup was pressurized to 1450 psi, keeping the overburden pressure 500 psi higher than the test pressure, and at test temperature

Table 2 Dimensions and petrophysical properties of the glass-bead pack

Length, in.	Diameter, in.	Pore volume, mL	Porosity, %	Permeability, D
13	0.18	1.625	30	17.1

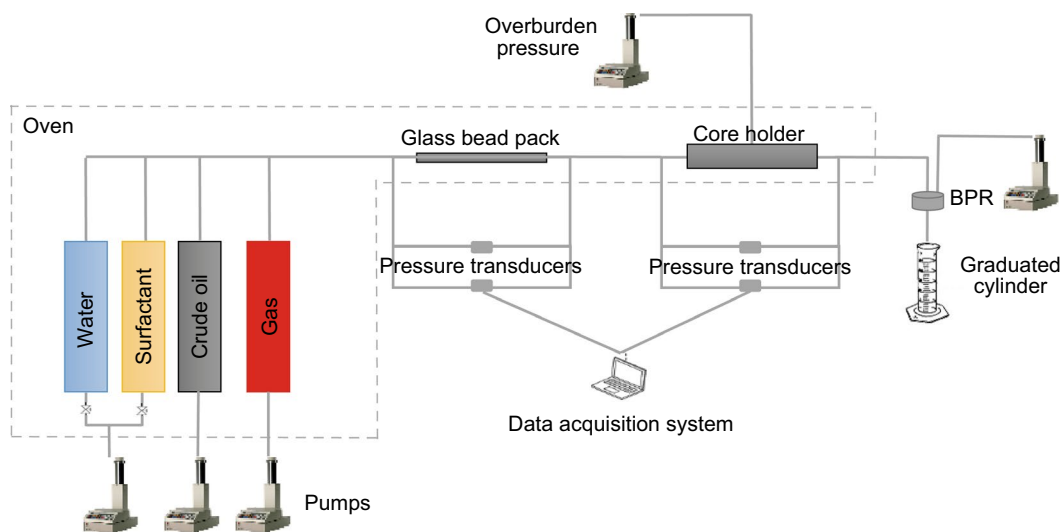


Fig. 1 Schematic of an experimental setup for mobility reduction evaluation and core flooding

of 50 °C. Once the pressure and temperature were stable, crude oil was injected at a flow rate of 5 ft/day until no more water was observed in the effluent. The water produced from the core sample was collected in a graduated cylinder for the original oil in place (OOIP) estimation. Then, water flooding was applied by injecting 5 PV of 10,000 ppm brine at a flow rate of 5 ft/day until no more oil was observed in the effluent. The high amount of water injection was to ensure that the optimum oil recovery by waterflooding was achieved, no more oil was produced by water injection, and the end effects would be diminished. Then, the second stage was to inject 1–1.5 PV of the surfactant solution (surfactant pre-flush) to mitigate the surfactant adsorption on the rock. After that, 5 PV of simultaneous injection of the surfactant solution and ScCO₂ was applied for 24 h at a flow rate of 5 ft/day. The pressure drop was recorded for the three oil recovery stages. Figure 1 shows the schematic diagram of the setup for the core flooding experiments. One baseline experiment was conducted by injecting ScCO₂ only for comparison purposes with oil recovery of CNF and AOS foam floods. Table 3 shows the properties for the Bentheimer sandstone samples used to conduct the core flooding experiments and the experimental conditions.

4 Results and discussion

4.1 Static foam test results

Foaming ability (or foamability) was investigated by measuring the initial foam heights h_{fi} for both surfactants from the shaking tests. Both surfactants gave almost the same initial foam column length h_{fi} . Therefore, both CNF and AOS are good foaming agents in terms of foaming ability. This also indicates the efficiency of both surfactants to reduce the air–liquid surface tension. The surface tension at the air–liquid interface will be discussed shortly.

Figure 2 shows the foam half-life for both surfactants at different salinities of 0 (deionized water), 10,000, 20,000, and 30,000 ppm. Both surfactants provided good foam stability. As observed, the foam stability decreases as the salinity increases at the salinity of 0–20,000 ppm, which is attributed to a reduction in repulsive forces between the surfactant molecules due to the addition of salts.

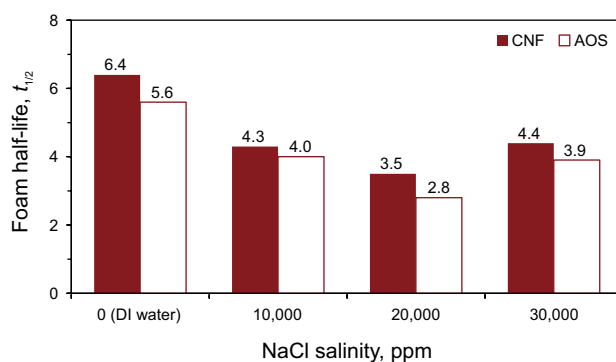


Fig. 2 Foam half-lives for both surfactants (0.5 wt%) in deionized water, 10,000, 20,000, and 30,000 ppm NaCl solutions

Moreover, CNF surfactant is slightly better than AOS at any salinity (0–30,000 ppm). For both surfactants, the stability of foam prepared with deionized water is the best. In addition, both surfactants exhibit an enhancement of foam stability at the salinity of 30,000 ppm. Liu et al. (2005) reported that the foam stability with CO₂ decreased with increasing salinity up to 2 wt%. Then, a further increase in salinity enhanced the foam stability. However, the foam stability plateaued shortly with further increase in salinity.

The foam stability with crude oil was impressive for both surfactants. The foam half-life for CNF lasted for more than 24 h and 12–18 h for AOS. Figure 3a shows images for CNF and Fig. 3b for AOS. The images were taken after 24 h for CNF foams and after 18 h for AOS foams. Each image shows samples in DI water, 10,000 and 20,000 ppm salinity left to right. Clearly, both surfactants produced stable foam with crude oil, but CNF foam was significantly stronger than that of AOS in the presence of crude oil.

However, shaking involves eventually very high shear rates which provide high energy for any surfactant to give its optimum performance as foaming agent regardless of how the shaking was performed. Therefore, it is difficult to recognize the differences in foaming ability and foam stability as well. Therefore, combining the shaking test observations with the interfacial tension measurements is next.

Table 3 Petrophysical properties of the sandstone cores and the experimental conditions in core flooding experiments

Run No.	Surfactant	Core length, in.	Core diameter, in.	Core pore volume, mL	Core porosity, %	Core permeability, D	Experiment type
1	–	12	1	33.52	21.71	1.87	Baseline
2	AOS	12	1	34.74	22.50	1.71	Foam flood
3	CNF	12	1	33.74	21.85	1.91	Foam flood

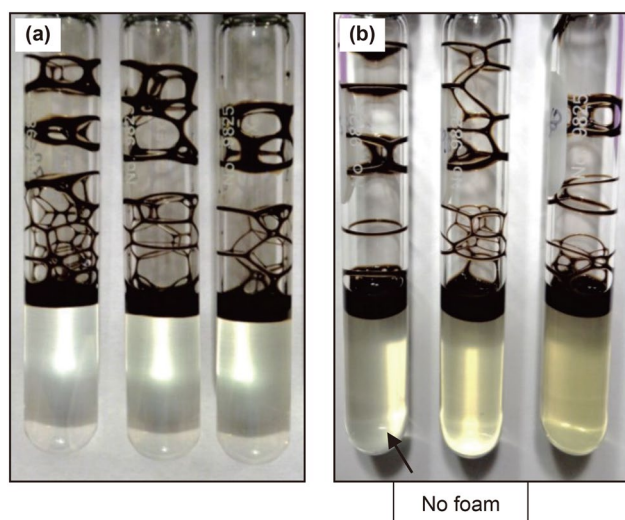


Fig. 3 **a** Images of CNF foam after 24 h and **b** images of AOS foam after 18 h, both foam samples at 0.5 wt% surfactant concentration and at a salinity of 0 (deionized water), 10,000 and 20,000 ppm from left to right

4.2 Interfacial tensions

As mentioned earlier, surface tensions were measured for different concentration samples prepared with deionized water and the measured results are shown in Fig. 4. The critical micelle concentrations (CMCs) for CNF and AOS are 0.011 wt% and 0.028 wt%, respectively. The surfactant concentration for foam applications is recommended above the CMC (Nikolov et al. 1986). Using the surfactant concentration above the CMC provides the best foam stability, whereas foam has less opportunity to be of good stability when the surfactant concentration is below the CMC (Rafati et al. 2012). The CMC defines the foaming efficiency of the surfactants. The lower the CMC is, the higher the foaming efficiency (Rosen and Kunjappu 2004). Moreover, Manhardt et al. (2000) found that the foaming ability decreased

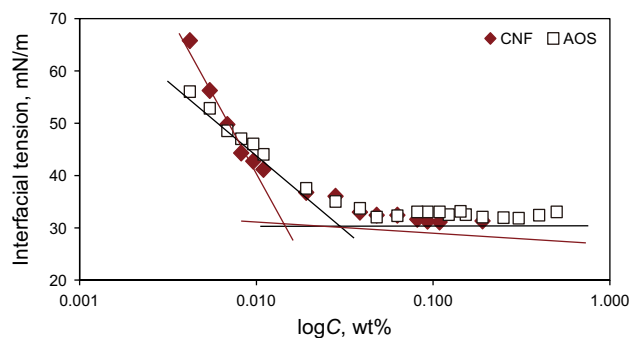


Fig. 4 Interfacial measurements for AOS and CNF (C is the surfactant concentration, wt%)

with a decrease in the surfactant concentration and no foam was generated at surfactant concentration below its CMC. Therefore, the lower the CMC of the surfactant is the better from different perspectives such as lowering the cost of the project due to the use of low surfactant concentrations without compromising the foaming efficiency.

According to Gibbs surface adsorption equation (Eq. 8), the higher the slope is, the higher the adsorption of the surfactant at the liquid–air interface, and consequently, the better the foamability and foam stability (Rosen and Kunjappu 2004). This is because the higher the adsorption at the air–liquid interface is, the smaller the area/molecule and the stronger the packing of the molecules at the interface (Rosen and Kunjappu 2004).

$$\Gamma = -\frac{1}{RT} \left(\frac{d\gamma}{d \ln C} \right) \quad (8)$$

where Γ is the surfactant adsorption at the air–liquid interface, R is the gas constant, T is temperature, γ is the surface tension, and C is the surfactant concentration.

Furthermore, for concentrations above 0.007 wt% in Fig. 4, CNF is able to reduce the interfacial tension lower than that of AOS which also indicates that CNF is predicted to perform better than AOS in foam generation. Table 4 shows the air–water and oil–water interfacial tensions for both 0.5 wt% surfactant solutions at different salinities.

4.3 Foam stability in the presence of crude oil

As shown in Table 4, the $\sigma_{o/w}$ for both surfactants dropped with the addition of salts (from deionized water to 10,000 ppm salinity), but no influence was observed on $\sigma_{o/w}$ with increasing the salinity. This shows that both surfactants would probably perform efficiently in the presence of oil, but CNF had higher $\sigma_{o/w}$ which suggests that it is better in terms of foam–oil tolerance.

Table 5 shows the entering, spreading, bridging coefficients, and lamellae number, respectively. The entering coefficient gives positive values for all surfactant solutions,

Table 4 Interfacial tensions $\sigma_{a/w}$ and $\sigma_{o/w}$ for AOS and CNF (0.5 wt%) at 23 °C

Salinity of surfactant solution (water phase), ppm	IFT between gas (or oil) and AOS solution, mN/m		IFT between gas (or oil) and CNF solution, mN/m	
	$\sigma_{a/w}$	$\sigma_{o/w}$	$\sigma_{a/w}$	$\sigma_{o/w}$
0 (deionized water)	32.50	1.40	30.70	5.88
10,000	32.30	0.52	31.00	3.94
20,000	32.10	0.44	31.25	3.51
30,000	32.15	0.38	31.11	3.11

Table 5 Entering, spreading, bridging coefficients, and lamellae number at 0.5 wt% surfactant concentration at 23 °C

Salinity of surfactant solution (water phase), ppm	Entering coefficient		Spreading coefficient		Bridging coefficient		Lamellae number	
	AOS	CNF	AOS	CNF	AOS	CNF	AOS	CNF
0 (Prepared with deionized water)	2.40	5.08	− 0.40	− 6.68	65.96	− 15.19	3.48	0.78
10,000	1.32	3.44	0.28	− 4.44	51.31	− 15.73	9.32	1.18
20,000	1.04	3.26	0.16	− 3.76	38.35	− 3.37	10.94	1.34
30,000	1.03	2.72	0.27	− 3.50	41.52	− 14.75	12.69	1.50

which clarifies that oil will enter the lamellae. However, the spreading coefficient implies that oil will spread at the air–water interface to destabilize AOS foams in saline solutions only. The spreading coefficient for CNF is negative for all samples. Moreover, the bridging coefficient gives negative values for CNF at all conditions. These observations imply that CNF is going produce very stable foam with oil. However, AOS produces stable foam with oil when the surfactant prepared with deionized water. Furthermore, lamellae number values confirm the same conclusions. The CNF foam is stable in deionized water and semi-stable in saline solutions, whereas AOS is semi-stable in deionized water and unstable in saline solutions.

4.4 Mobility reduction evaluation in the high-permeability glass-bead pack

Table 6 shows the results for 16 runs on the high-permeability glass-bead pack at high and low shear rates for both surfactants with ScCO₂ foam. Moreover, one baseline experiment was conducted with ScCO₂ injection only and resulted in a very low steady-state pressure drop (0.04 psi) which corresponds with 0.03 cP effective viscosity. The average of the recorded steady-state pressure drop data were used to calculate the mobility, foam effective viscosity, and mobility reduction factor. Experimental conditions and results for these tests are listed in Table 6.

Figure 5 shows the effect of three injection qualities on the viscosities of both surfactants at the high shear rate in deionized water. The AOS foam viscosity decreased but the CNF foam viscosity increased as the injection quality decreased. The opposite behavior of these foaming agents

Table 6 Experimental conditions and results for AOS and CNF with CO₂ in glass-bead packs

Run No.	Surfactant ^a	Salinity, ppm	Injection quality, %	Flow rate <i>q</i> , mL/min	Shear rate, s ^{−1}	Steady-state pressure drop Δ <i>P</i> _{ss} , psi	Mobility λ, mD/cP	Effective viscosity μ _{eff} , cP	Mobility reduction factor <i>f</i> _{mr}
1	AOS	0	90	0.5	317	208	118	145	−
2	AOS	10,000	90	0.5	317	164	150	114	4100
3	AOS	20,000	90	0.5	317	161	156	109	−
4	AOS	30,000	90	0.5	317	216	459	37	−
5	AOS	0	70	0.5	317	175	142	121	−
6	AOS	10,000	70	0.5	317	99	249	69	2475
7	AOS	20,000	70	0.5	317	93	265	64	−
8	AOS	30,000	70	0.5	317	91	273	63	−
9	AOS	0	50	0.5	317	122	202	85	−
10	AOS	10,000	90	0.015	9.51	9.97	74	230	250
11	CNF	0	90	0.5	317	162	153	112	−
12	CNF	0	70	0.5	317	207	119	143	−
13	CNF	0	50	0.5	317	225	109	154	−
14	CNF	10,000	90	0.5	317	178	138	123	4450
15	CNF	10,000	90	0.015	9.51	16	46	371	400
16	−	10,000	−	0.5	317	0.04	−	0.03	−

^aThe surfactant concentrations were 0.5 wt% in runs 1–15. No surfactant was used in the baseline experiment (run 16)

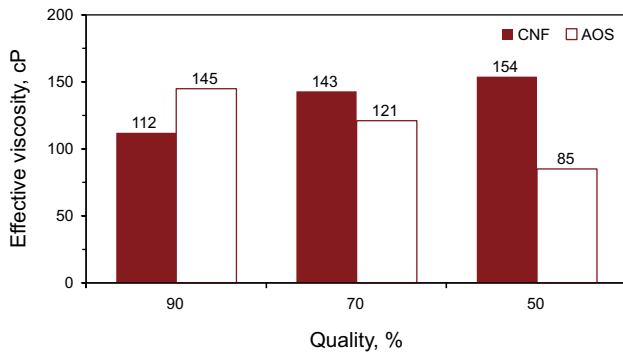


Fig. 5 Effect of injection quality on the effective viscosities of AOS and CNF (0.5 wt% in deionized water) foams in the glass-bead pack at a high shear rate of 317 s^{-1}

can be attributed to many reasons that were not covered in this study. In fact, the relationship of the foam viscosity with injection quality is still controversial. In an experimental study conducted by Marsden and Khan (1966), they found that the higher the injection quality is, the higher the foam viscosity. Lee and Heller (1990) experimentally concluded that the increase in injection quality decreased the viscosity. The foam viscosity depends on flow rate, permeability of the porous media, and foam texture (Hirasaki and Lawson 1985).

The effect of shear rate (317 and 9.51 s^{-1}) on the effective viscosities of both AOS and CNF foams at 90% injection quality and 10,000 ppm salinity are shown in Fig. 6. The higher the shear rate resulted in the lower viscosity because of the shear thinning nature of the foam. As shown in Fig. 6, the viscosities of CNF foam at both shear rates are higher than that of the AOS foam.

Figure 7 also shows all results for CNF and AOS foams (0.5 wt%, 10,000 ppm salinity) at a low shear rate of 9.51 s^{-1} and 90% injection quality. Again, the CNF foam proves powerful performance with higher steady-state pressure drop,

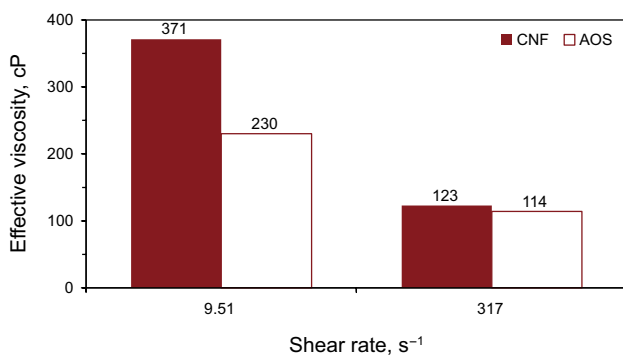


Fig. 6 Effect of shear rate on the effective viscosities of AOS and CNF foams at 0.5 wt% surfactant concentration and 90% injection quality

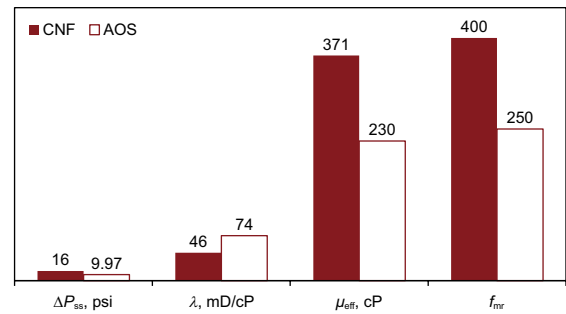


Fig. 7 Comparison of experimental results at low shear rate between AOS and CNF foams (0.5 wt%, 10,000 ppm salinity) with ScCO_2 at 90% injection quality

lower mobility, higher foam viscosity, and higher mobility reduction factor.

4.5 Mobility reduction evaluation in low-permeability Bentheimer sandstone cores

Two baseline runs were conducted using N_2 injection at 850 psi and ScCO_2 injection at 1800 psi for comparison. All experimental conditions and results are listed in Table 7.

The effect of permeability is shown in Fig. 8 which compares the foam viscosities for AOS and CNF with ScCO_2 at 90% injection quality at a shear rate of 9 s^{-1} . The permeabilities of the cores and the glass-bead pack are 1.62–1.80 Darcy (Table 7) and 17.1 Darcy (Table 2), respectively. CNF is repeatedly proved to be better than AOS by generating higher foam viscosity in both cases at high and low-permeability porous media. The results in Fig. 8 are in agreement with the fact that foam favors the higher permeability porous media. The viscosities of surfactant foams in the glass-bead pack are extremely higher than that in sandstone cores.

The effect of injection quality at low-permeability sandstone cores was investigated using two injection qualities 90% and 70% for both surfactants with ScCO_2 at a shear rate of 9.51 s^{-1} . The pressure drop curves for both surfactant foams are shown in Fig. 9 for 90% injection quality and Fig. 10 for 70% injection quality. According to the pressure profiles, the CNF foam is stronger at 90% injection quality, whereas the AOS foam is stronger at 70% injection quality. Therefore, the results suggest that CNF is better at more realistic conditions (i.e., low shear rate and sandstone reservoirs), CNF co-injection with ScCO_2 provides higher foam viscosity at higher injection qualities, while AOS requires low injection qualities for better performance. This also indicates that using CNF with ScCO_2 for foam mobility control will eventually reduce the cost as the amount of liquid decreases as the injection quality increases.

Table 7 Experimental conditions and results for AOS and CNF in sandstone cores

Run No.	Surfactant	Gas	Pressure P, psi	Velocity, ft/day	Shear rate, s ⁻¹	Injection quality, %	Pore volume, mL	Permeability k, D	Steady-state pressure drop ΔP _{ss} , psi	Mobility λ, mD/cP	Foam effective viscosity, cP	Mobility reduction factor f _{mr}
1	AOS	SeCO ₂	1800	5	8.77	90	31.24	1.70	0.40	411	4.13	1.67
2	AOS	SeCO ₂	1800	5	9.30	70	33.74	1.58	25.42	6.79	232.8	105.9
3	CNF	SeCO ₂	1800	5	9.10	90	34.74	1.70	0.60	301	5.65	2.5
4	CNF	SeCO ₂	1800	5	8.92	70	34.74	1.78	2.00	89	20	8.3
5	AOS	N ₂	850	5	9.15	90	34.24	1.65	1.35	130	12.7	3.4
6	AOS	N ₂	850	10	18.31	90	34.24	1.65	3.46	100	18	8.6
7	CNF	N ₂	850	5	8.76	90	34.24	1.80	12.89	13.61	121.23	32.2
8	CNF	N ₂	850	10	17.53	90	34.24	1.80	34.4	10.20	176.5	86
9	-	N ₂	850	5	9.05	-	33.74	1.62	0.40	680	0.04	-
10	-	SeCO ₂	1800	5	8.83	-	32.74	1.70	0.24	-	-	-

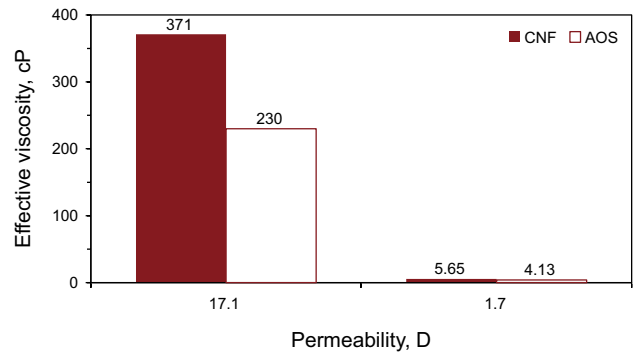


Fig. 8 Effect of permeability on effective viscosity of AOS and CNF foams (0.5 wt%, 10,000 ppm salinity) with SeCO₂ at 90% injection quality

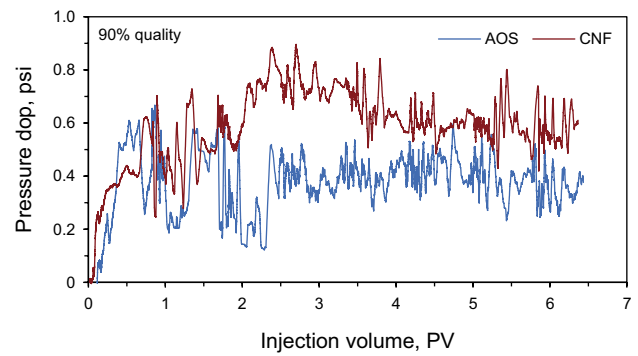


Fig. 9 Pressure drop curves for AOS and CNF foams (with SeCO₂) at 90% injection quality in sandstone cores

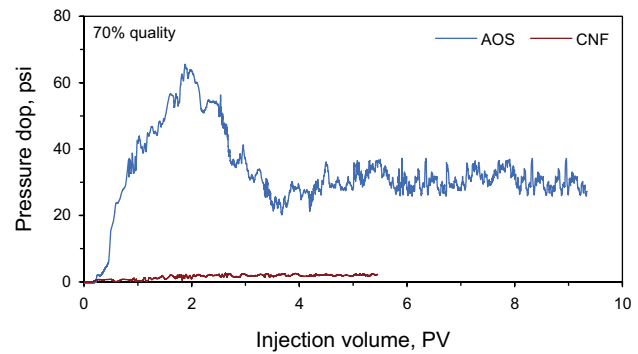


Fig. 10 Pressure drop curves for AOS and CNF foams (with SeCO₂) at 70% injection quality in sandstone cores

The mobility control with N₂ gas was also tested for both surfactants. The pressure profiles for AOS and CNF are shown in Fig. 11. These experiments were conducted on sandstone core samples at two velocities of 5 and 10 ft/day (9 and 18 s⁻¹) with an injection quality of 90%. In these experiments, the surfactant solutions used had a concentration of 0.5 wt%, which were prepared with 10,000 ppm NaCl

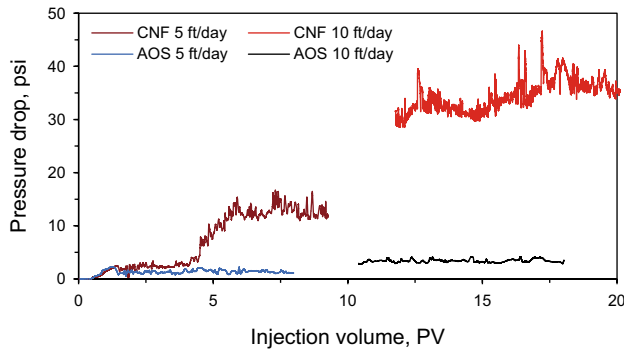


Fig. 11 Pressure drop curves for AOS and CNF foams with N_2 at different injection velocities (90% injection quality, 850 psi injection pressure)

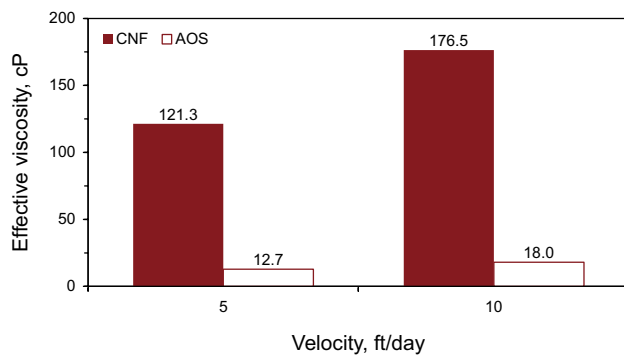


Fig. 12 Foam effective viscosity in sandstone cores for CNF and AOS foams with N_2 gas at different injection velocities (90% injection quality, 850 psi injection pressure)

solution. Each surfactant solution was injected simultaneously with N_2 gas at 5 ft/day until the steady-state pressure drop was reached, then the velocity was raised to 10 ft/day until the steady-state pressure drop was reached for the new velocity. From Fig. 11, the CNF foam appeared always better in terms of flow resistance at both velocities than the AOS foam. Moreover, Fig. 12 compares the foam viscosities for AOS and CNF at both velocities. Surprisingly, the viscosity increases as the velocity (i.e., shear rate) increases for both foams. Although this is shear thickening behavior, foam is known of its non-Newtonian shear thinning nature (Schramm and Wassmuth 1994). This behavior could be related to the procedure of the experimental work. At 5 ft/day, the foam was very efficient to provide high flow resistance due to the gas blockage effect. Therefore, the gas relative permeability is already low, and increasing the velocity to 10 ft/day at such conditions would promote the foam generation because of the high shear rate in a blocked porous media. As a result, foam contradicted its shear thinning nature by providing higher viscosity at higher shear rates, lesson learned.

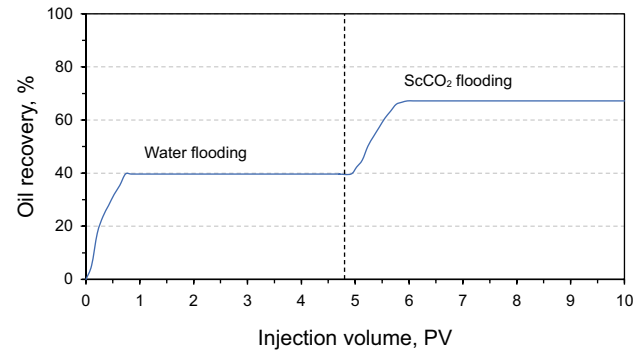


Fig. 13 Oil recovery of the baseline experiment

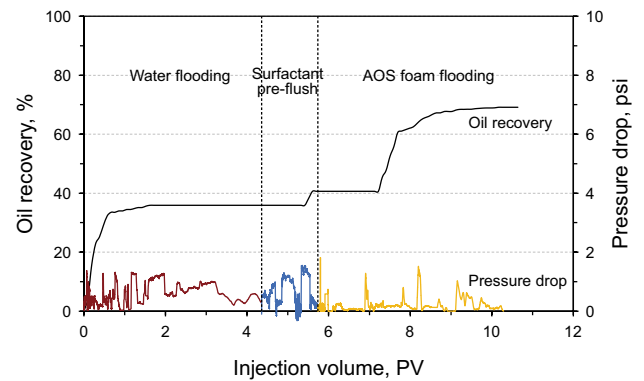


Fig. 14 Oil recovery and pressure drop curves across the sandstone core for waterflooding, AOS surfactant (0.5 wt% and 10,000 ppm salinity) pre-flush, and AOS surfactant with $ScCO_2$ foam flood at 90% injection quality

4.6 Core flooding experiments

The oil recovery from the baseline experiment is shown as a function of pore volume injected in Fig. 13. The ultimate oil recovery of water flooding is 39% of OOIP. The water flooding was followed by 5–6 PV of continuous $ScCO_2$ injection which resulted in 27.54% OOIP more oil recovery. The total oil recovery from the baseline experiment is 66.54% of the OOIP.

Figure 14 shows the results for AOS as a foaming agent after water flooding. The same procedure was conducted. This run started with injecting 4.56 PV water flooding, which resulted in an oil recovery of 35.42% of the OOIP. Then, 1.62 PV of the AOS surfactant solution was injected to reduce the surfactant adsorption on the rock surfaces. The surfactant pre-flush stage resulted in an oil recovery of 4.75% of the OOIP. The third stage was the foam flood with simultaneous injection of 5 PV of AOS- $ScCO_2$. The AOS foam flood resulted in an additional oil recovery of 28.5%. Then, the total oil recovery was 68.67% of the

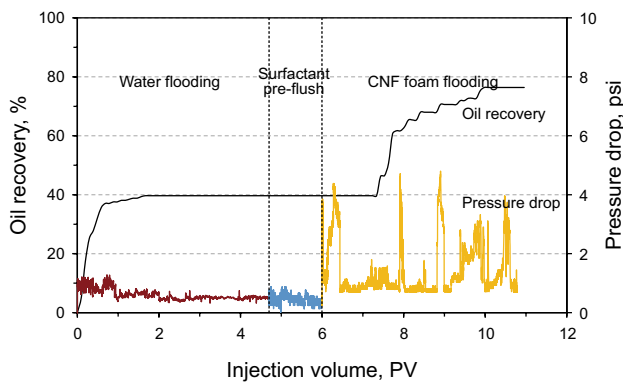


Fig. 15 Oil recovery and pressure drop curves across the sandstone core for waterflooding, CNF surfactant (0.5 wt% and 10,000 ppm salinity) pre-flush, and CNF surfactant with ScCO₂ foam flood at 90% injection quality

OOIP. The additional recovery by AOS foam accounted for 1% higher than that of baseline experiment.

CNF foam core flood results are shown in Fig. 15. Water flooding stage produced an oil recovery of 39.66% of the OOIP. Moreover, no oil production was observed during the surfactant pre-flush stage in which 1.5 PV of CNF surfactant solution was injected to reduce the adsorption effect. The final stage, CNF-ScCO₂ simultaneous injection or foam flooding resulted in a recovery of 36.3% of the OOIP after water flooding. The amount of oil produced by the CNF foam was 7.87% higher than that by the AOS foam and 8.83% higher than the baseline experiment. The total recovery for this core flood was 75.96%.

5 Conclusions

- (1) Both AOS and CNF surfactants show good foaming ability and foam stability without oil in shaking tests. Such behavior is not representative to the actual foaming ability of both surfactants because the shaking tests are naturally involved high shear rate which enforces the surfactants to perform at their optimum abilities as foaming agents. However, CNF was able to reduce the air–water interfacial tension lower than that of AOS.
- (2) The newly developed surfactant, CNF, shows impressive foam oil tolerance than AOS. It does not reduce the oil–water interfacial tension to low value as with AOS in saline solutions. This makes it a good surfactant for the applications of foam for mobility control.
- (3) CNF provides negative values of entering, spreading, and bridging coefficients, whereas AOS provides negative values in deionized water only. Moreover, the lamellae number indicates that the CNF foam is stable in deionized water and semi-stable with the addition

of salts in terms of foam–oil tolerance. However, the lamellae number for AOS shows semi-stable in deionized water and unstable at all salinities. These results show that CNF foam is very stable with oil more than AOS foam.

- (4) At 90% injection quality, the mobility reduction with ScCO₂, and with N₂ at lower pressures, CNF shows higher foam viscosity and better mobility reduction than AOS.
- (5) For oil recovery, AOS foam produced 1% more than the baseline experiment, whereas CNF foam produced almost 7.87% more than AOS foam, and 8.38% more than the baseline experiment.
- (6) It is not recommended to investigate foam viscosity at more than one shear rate during one experiment. Testing two shear rates in series in one experiment would provide erroneous results. In this study, measuring the foam viscosity at two shear rates in one experiment resulted in shear thickening foam behavior, while foam is non-Newtonian shear thinning in nature.

Open Access This article is licensed under a Creative Commons Attribution 4.0 International License, which permits use, sharing, adaptation, distribution and reproduction in any medium or format, as long as you give appropriate credit to the original author(s) and the source, provide a link to the Creative Commons licence, and indicate if changes were made. The images or other third party material in this article are included in the article’s Creative Commons licence, unless indicated otherwise in a credit line to the material. If material is not included in the article’s Creative Commons licence and your intended use is not permitted by statutory regulation or exceeds the permitted use, you will need to obtain permission directly from the copyright holder. To view a copy of this licence, visit <http://creativecommons.org/licenses/by/4.0/>.

References

Adkins S, Chen X, Nguyen Q, Sanders A, Johnston K. Effect of branching on the interfacial properties of nonionic hydrocarbon surfactants at the air–water and carbon dioxide–water interfaces. *J Colloid Interface Sci.* 2010;346(2):455–63. <https://doi.org/10.1016/j.jcis.2009.12.059>.

Boeije C, Bennetzen M, Rossen W. A methodology for screening surfactants for foam enhanced oil recovery in an oil-wet reservoir. *SPE Res Eval Eng.* 2017;20(04):795–808. <https://doi.org/10.2118/185182-PA>.

Denkov N. Mechanisms of foam destruction by oil-based antifoams. *Langmuir.* 2004;20(22):9463–505. <https://doi.org/10.1021/la049676o>.

Dicksen T, Hirasaki G, Miller C. Conditions for foam generation in homogeneous porous media. In: *SPE/DOE improved oil recovery symposium*, 13–17 April, Tulsa, Oklahoma; 2002. <https://doi.org/10.2118/75176-MS>.

Enick R, Olsen D, Ammer J, Schuller W. Mobility and conformance control for CO₂ EOR via thickeners, foams, and gels—a literature review of 40 years of research and pilot tests. In: *SPE improved oil*

- recovery symposium, 14–18 April, Tulsa, Oklahoma, USA; 2012. <https://doi.org/10.2118/154122-MS>.
- Farajzadeh R, Andrianov A, Zitha P. Investigation of immiscible and miscible foam for enhancing oil recovery. *Ind Eng Chem*. 2010;49(4):1910–9. <https://doi.org/10.1021/ie901109d>.
- Fried A. The foam-drive process for increasing the recovery of oil. Washington, DC: U.S. Bureau of Mines, Rep. Inv., 5866; 1961.
- Green D, Willhite G. Enhanced oil recovery. Volume 6, SPE Textbook Series. Richardson, Texas: SPE; 1998.
- Harkins W. A general thermodynamic theory of the spreading of liquids to form duplex films and of liquids or solids to form monolayers. *J Chem Phys*. 1941;9(7):552–68. <https://doi.org/10.1063/1.1750953>.
- Haugen Å, Fernø M, Graue A, Bertin H. Experimental study of foam flow in fractured oil-wet limestone for enhanced oil recovery. *SPE Res Eval Eng*. 2012;15(02):218–28. <https://doi.org/10.2118/129763-PA>.
- Healy R, Holstein E, Batycky J. Status of miscible flooding technology. In: 14th world petroleum congress, 29 May–1 June, Stavanger, Norway; 1994.
- Hirasaki G, Lawson J. Mechanisms of foam flow in porous media: apparent viscosity in smooth capillaries. *SPE J*. 1985;25(02):176–90. <https://doi.org/10.2118/12129-PA>.
- Lee H, Heller J. Laboratory measurements of CO₂-foam mobility. *SPE Res Eng*. 1990;5(02):193–7. <https://doi.org/10.2118/17363-PA>.
- Li R, Hirasaki G, Miller C, Masalmeh S. Wettability alteration and foam mobility control in a layered, 2D heterogeneous sandpack. *SPE J*. 2012;7(04):1207–20. <https://doi.org/10.2118/141462-PA>.
- Liu Y, Grigg R, Bai B. Salinity, pH, and surfactant concentration effects on CO₂-foam. In: SPE international symposium on oilfield chemistry, 2–4 February, The Woodlands, Texas; 2005. <https://doi.org/10.2118/93095-MS>.
- Mannhardt K, Novosad J, Schramm L. Comparative evaluation of foam stability to oil. *SPE Res Eval Eng*. 2000;3(01):23–34. <https://doi.org/10.2118/60686-PA>.
- Marsden S, Khan S. The flow of foam through short porous media and apparent viscosity measurements. *SPE J*. 1966;6(01):17–25. <https://doi.org/10.2118/1319-PA>.
- Nikolov A, Wasan D, Huang D, Edwards D. The effect of oil on foam stability: mechanisms and implications for oil displacement by foam in porous media. In: SPE annual technical conference and exhibition, 5–8 October, New Orleans, Louisiana; 1986. <https://doi.org/10.2118/15443-MS>.
- Porter MR. Handbook of surfactants. London: Blackie Academic & Professional; 1994.
- Rafati R, Hamidi H, Idris A, Manan M. Application of sustainable foaming agents to control the mobility of carbon dioxide in enhanced oil recovery. *Egypt J Pet*. 2012;21(2):155–63. <https://doi.org/10.1016/j.ejpe.2012.11.010>.
- Robinson J, Woods W. A method of selecting foam inhibitors. *J Soc Chem Ind*. 1948;67(9):361–5. <https://doi.org/10.1002/jctb.5000670908>.
- Rosen M, Kunjappu J. Foaming and antifoaming by aqueous solutions of surfactants and interfacial phenomena. Hoboken: Wiley; 2004. p. 308–35.
- Schramm L. Surfactants: fundamentals and applications in the petroleum industry. Cambridge: Cambridge University Press; 2000. p. 3–50.
- Schramm L, Novosad J. Micro-visualization of foam interactions with a crude oil. *Colloids Surf*. 1990;46(1):21–43. [https://doi.org/10.1016/0166-6622\(90\)80046-7](https://doi.org/10.1016/0166-6622(90)80046-7).
- Schramm L, Wassmuth F. Foams: basic principles foams: fundamentals and applications in the petroleum industry, vol. 242. Washington: American Chemical Society; 1994. p. 3–45.
- Taber J, Martin F, Seright R. EOR screening criteria revisited—Part 1: introduction to screening criteria and enhanced recovery field projects. *SPE Res Eng*. 1997;12(03):189–98. <https://doi.org/10.2118/35385-PA>.
- Talley L. Hydrolytic stability of alkylethoxy sulfates. *SPE Res Eng*. 1988;3(01):235–42. <https://doi.org/10.2118/14912-PA>.